Electrochemical oxidation of syngas on nickel and ceria anodes

Tabish, A. N.; Patel, H. C.; Purushothaman Vellayani, A.

DOI
10.1016/j.electacta.2017.01.074

Publication date
2017

Document Version
Accepted author manuscript

Published in
Electrochimica Acta

Title: Electrochemical Oxidation of Syngas on Nickel and Ceria Anodes

Author: A.N. Tabish H.C. Patel P.V. Aravind

PII: S0013-4686(17)30074-9
DOI: http://dx.doi.org/doi:10.1016/j.electacta.2017.01.074
Reference: EA 28741

To appear in: *Electrochimica Acta*

Received date: 27-9-2016
Revised date: 5-1-2017
Accepted date: 12-1-2017

Please cite this article as: A.N. Tabish, H.C. Patel, P.V. Aravind, Electrochemical Oxidation of Syngas on Nickel and Ceria Anodes, *<![CDATA[Electrochimica Acta]]>* (2017), http://dx.doi.org/10.1016/j.electacta.2017.01.074

Link to formal publication (Elsevier): http://dx.doi.org/doi:10.1016/j.electacta.2017.01.074

Electrochemical Oxidation of Syngas on Nickel and Ceria Anodes

A.N. Tabish[a,b,*], HC. Patel[a], PV. Aravind[a]

[a]*Department of Process and Energy (Energy Technology), Delft University of Technology, 2628CB Delft, The Netherlands*
[b]*Department of Chemical Engineering, University of Engineering and Technology Lahore, Pakistan*

Abstract

Fuel flexibility of solid oxide fuel cells enables the use of low cost and practical fuels like syngas. Understanding of the oxidation kinetics with syngas is essential for proper selection of anode material and its design optimization. Using nickel and ceria pattern anodes, we study the electrochemical oxidation of syngas in both dry and wet environments. In dry environment, the polarization resistance of CO oxidation drops drastically with the addition of small amounts of hydrogen to CO gas stream. In wet environment (4 % moisture), the polarization resistance of CO is only slightly higher than syngas and hydrogen. Observation in the first case is related to the hydrogen preferential oxidation whereas latter is a combined effect of water gas shift reaction and preferential oxidation of hydrogen. Kinetic modeling is also carried out to understand hydrogen and CO co-oxidation. Simulation suggests that CO, besides hydrogen, may also electrochemically oxidize depending upon its concentration in the syngas. At higher concentration, CO electrochemical oxidation may be non-negligible especially in case of ceria anodes.

Keywords: pattern anodes, SOFC, syngas, elementary modeling, ceria

1. Introduction

Solid oxide fuel cells (SOFCs) are considered as promising candidates for next generation stationary power production because they are efficient and fuel flexible. Besides hydrogen, various hydrocarbon based fuels such as biomass and coal derived synthetic gas (syngas), natural gas, and biogas etc. are suggested as potential fuels for SOFC as they can be fed directly to the anode after necessary cleaning [1, 2, 3, 4]. Syngas is mainly a mixture of hydrogen, CO and varying concentrations of CH_4, H_2O, CO_2, N_2 and other impurities. Natural gas and biogas can also be reformed to produce a mixture of hydrogen and CO. Thus in

*Corresponding author
Email address: a.nadeemtabish@tudelft.nl (A.N. Tabish)

all these fuels, a mixture of hydrogen and CO is ultimately expected to undergo electrochemical oxidation. When CO/H_2 mixture is fed to SOFC anode, overall (electro-)chemical reactions can be described using the Kroger-Vink notation:

$$H_2 + O_O^x \rightarrow H_2O + V_O^{\bullet\bullet} + 2e^t \quad (1)$$

$$CO + O_O^x \rightarrow CO_2 + V_O^{\bullet\bullet} + 2e^t \quad (2)$$

$$CO + H_2O \leftrightarrow CO_2 + H_2 \quad (3)$$

Here O_O^x is a regular oxide ion and has no effective charge (x) and the oxide ion vacancy, $V_O^{\bullet\bullet}$, has an effective charge +2.

Total faradaic current is a result of charge transfer reactions 1 and 2. The relative contribution of both of these reactions is not very clear so far. Several experimental [5, 6, 7, 8, 9] and modeling [10, 11, 12, 13, 14, 15] studies have been conducted to understand the effect of syngas composition on the cell performance. For example, at low CO concentrations, even up to equimolar CO/H_2 mixture, cell performance is almost the same as obtained by moist hydrogen [6]. Sasaki [8] reported only 4 % drop in the cell voltage for CO/H_2 = 7:3 (at 1000 ^oC and 0.32 $A.cm^{-2}$) indicating only insignificant effect on the cell performance. Sukeshini [9] observed monotonous decrease in the maximum power density with increase in CO/H_2 ratio, and the degradation was not more than 25 % for CO/H_2 = 3:1. For very high CO fractions, CO/H_2 = 9:1, significant drop in the cell performance at 950 ^oC is reported [7]. These studies are conducted for short term operation and proved good performance for a wide range of CO/H_2 ratios.

It is known that the rate of electrochemical oxidation of CO is 2-3 times slower than that of hydrogen [5]. Thus, hydrogen is expected to oxidize preferentially in syngas mixtures [16]. It is worthwhile remembering that steam is the product of hydrogen oxidation which in turn promotes CO conversion via water-gas-shift (WGS) reaction (reaction 3) thus producing hydrogen. Whether CO electrochemically oxidizes as well, is very uncertain. In modeling studies, two different approaches are considered to address this concern. Firstly, it is commonly assumed that only hydrogen participates in electrochemical oxidation while CO is converted to hydrogen via WGS reaction. So total current density is solely attributed to electrochemical oxidation of hydrogen. Secondly, some authors [10, 12] have taken care of the current fraction from both CO and hydrogen oxidation on the basis of their electrochemical oxidation rates in CO/CO_2 and H_2/H_2O environments. Both of these approaches have their own limitations because of non-electrochemical oxidation of CO in first approach and linear coupling between hydrogen and CO electrochemistry in the latter. Recently, Bao et al.[11, 17] proposed a non-linear coupling of hydrogen and CO electrochemistry in order to correlate total current output with syngas composition. They developed a model based on macroscopic electrochemistry and species transport in complex microporous structure. There study concludes that as CO/H_2 ratio increases, hydrogen current fraction decreases which they

associated to the contribution of electrochemical oxidation of CO. However, as their work did not take into account the elementary reactions explicitly, further work is required to understand possible electrochemical oxidation of CO in syngas mixtures.

Using syngas as an SOFC fuel requires electromechanically stable anode materials besides high electrocatalytic activity. Practically viable anodes are expected to maximize the (electro-)chemical oxidation (reactions 1-3) and suppress coke formation and the influence of syngas contaminants like H_2S and HCl. The state-of-the-art Ni/YSZ anode fulfills most of the requirements related to catalysis and thus widely used in pure hydrogen feed. However, inherited poor redox stability of nickel [18] and carbon intolerance [19] make Ni/YSZ anodes less suitable for use in syngas. Recently ceria-based materials have gained considerable attention as possible alternative anodes for hydrocarbon feeds [20, 21]. In non-electrochemical applications, ceria has been extensively investigated as a support material for various reactions like hydrocarbon oxidation, WGS conversion, and CO preferential oxidation (CO-PROX) [22]. As an anode material, ceria has shown even better catalytic activity for hydrogen and CO oxidation compared to nickel [23, 16]. This superior activity of ceria is a result of extended reaction sites on ceria surface that are limited to geometrical interface between ionic and electronic phases in case of nickel anode. Conversely, the electronic conductivity and WGS catalytic activity of pure ceria is too low to be used as an anode in syngas environment [24, 25]. Electronic conductivity of ceria (0.2–2.0 $S.cm^{-1}$) is 3-4 orders of magnitude lower than that for nickel ($21.4x10^3$ $S.cm^{-1}$) at 1000 ^oC [26]. Thus the added advantages of both of these materials have been combined and tested for syngas applications with promising results compared to Ni/YSZ [27, 28]. Besides nickel/ceria cermet, copper/ceria cermet has also been tested in syngas with better performance than Ni/YSZ [29]. In copper/ceria cermet, copper primarily provides electronic conductivity to the anode and is otherwise catalytically inert [30]. While major focus of these studies was the development of better performing anode, very little attention has been paid on understanding the electrochemistry of fuel oxidation on ceria. Available knowledge of possible reaction mechanism(s), rate-limiting processes and WGS catalytic activity of ceria at cell operating temperature is very limited [16, 26, 31, 32, 33, 34] . Therefore, it is essential to investigate the reaction kinetics on nickel and ceria separately in order to realize the commercialization of nickel/ceria cermet anodes.

Studying reaction kinetics with porous and cermet structures has their own inherent disadvantages. For example, the gas diffusion impedance in case of symmetrical cells can be significant at low frequencies [35]. Since the objective of this work is to study the kinetics, all such effects arising out of geometrical parameters need to be avoided. Hence we use pattern cells where the geometry is well defined and the reactions can be localized. Since the current drawn is very small, the gas diffusion impedance is not expected to play any significant part in determining the response [23]. The spectra obtained are expected to be easier to analyze as well.

Previously, using nickel and ceria pattern cells, we mainly focused on the oxidation of CO/H_2 dry mixtures [36]. Results with pure hydrogen and CO [16] were also included for comparison. From these studies we concluded that hydrogen is preferentially oxidized in CO/H_2 mixtures. This conclusion was based on the observation that while adding small amounts of hydrogen to CO feed stream, impedance spectra were very close to that of pure hydrogen. In this work, we intend to extend the discussion using humidified syngas environment (4 % moisture). The results in humidified environment are compared with those obtained in dry environment. This sort of comparison between nickel and ceria anodes has not been reported before. Further, we developed an elementary kinetic model for CO/H_2 mixtures based on the previous models for pure hydrogen and CO oxidation in order to study the effect of WGS conversion and syngas compositions.

2. Experimental and modeling methodology

2.1. Cell preparation

Electrolyte supported, nickel and ceria pattern electrode cells are used in this study. Symmetrical cell configuration was chosen to study the anode processes. 8 % YSZ substrates (25 mm diameter and 250 μm thick) were obtained from Fuel cell materials (www.fuelcellmaterials.com). Nickel and ceria were deposited on to the substrates through a stainless steel mask using DC magnetron sputtering (AJA International, ATC 2600 UHV). Thickness of nickel and ceria patterns was 1.780 μm and 500 nm, respectively. Details of the sputtering process are reported previously [16, 37]. Figure 1 shows the schematic of the pattern cells. Area specific triple-phase-boundary (TPB) length of the cells is 0.203 $m.cm^{-2}$.

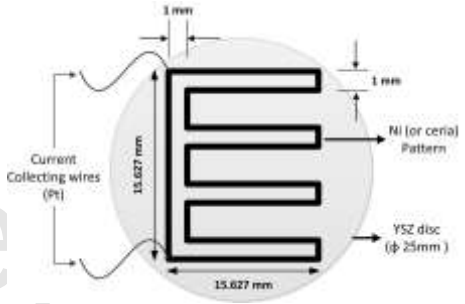

Figure 1: Schematic of Ni and ceria pattern cells

2.2. Cell test station

A schematic representation of quartz reactor tube containing ceramic cell holder is shown in figure 2. Cell was placed between two macro-porous ceramic supports also working as gas distributors. Gold mesh was applied on both sides of the cell for current collection. A small weight was placed on the top distributor

to ensure a good contact between gold mesh and the cell. Quartz tube was placed inside a temperature controlled furnace for testing at desired temperature. For humidified experiments, the gas mixtures were saturated in a temperature controlled humidifier.

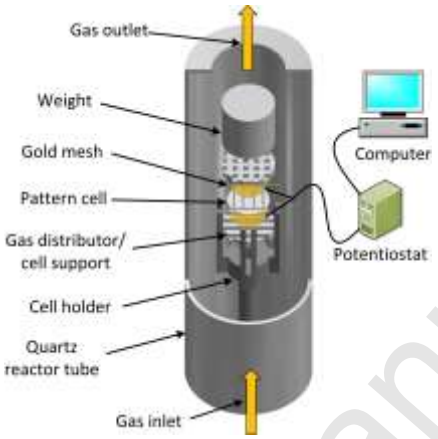

Figure 2: Cell test station

Electrochemical impedance spectroscopy was carried out to identify different processes affecting the cell operation using Gamry Potentiostat (R600). EIS measurements were conducted with AC perturbation of 10mV, between 700 ^{o}C to 850 ^{o}C and in a frequency range of 100 kHz to 0.01 Hz. In case of ceria, cells were exposed to 4 % moist hydrogen and sufficient time was given for reduction before impedance measurements. Gas compositions tested in this study are shown in table 1.

Gas environment	Fuel no.	Syngas composition			
		H_2 (%)	CO (%)	H_2 (%)	CO_2 (%)
Dry	F1	50	0	0	50
	F2	40	10	0	50
	F3	30	20	0	50
	F4	20	30	0	50
	F5	0	50	0	50
Wet	F6	96	0	4	0
	F7	72	24	4	0
	F8	48	48	4	0
	F9	28	68	4	0
	F10	0	96	4	0

Table 1: Fuel gas compositions tested in the study

2.3. Equivalent circuit model (ECM)

Impedance modeling was done by defining an appropriate equivalent circuit model [16, 38] as shown in figure 3. Two R-CPE elements connected in series with electrolyte resistance (*Re*) are associated to two dominant polarization processes i.e., a high-frequency process (R1-CPE1) and a low-frequency process (R2-CPE2). CPE is a constant-phase-element indicating a distributed capacitance. The impedance of this equivalent circuit (Z_{EC}) is defined as;

$$Z_{EC} = Re + \frac{R_1}{1 + R_1 Q_1 (i\omega)^{n_1}} + \frac{R_2}{1 + R_2 Q_2 (i\omega)^{n_2}} \quad (4)$$

Here, R_i [Ω] represent the resistances, and Q_i [$F s^{n-1}$] and n_i are the frequency-independent CPE parameters. Relaxation frequency (f_s) and the pseudo-capacitance (C_{eq}) of a process described by an R-CPE circuit are;

$$f_s = \frac{1}{2\pi \sqrt[n_i]{R_i Q_i}} \quad (5)$$

$$C_{eq} = \frac{\sqrt[n_i]{R_i Q_i}}{R_i} \quad (6)$$

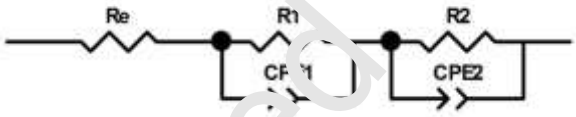

Figure 3: Equivalent circuit model (ECM)

2.4. Elementary kinetic model

The relevant equations for elementary kinetic modeling are given in table 2. Elementary reactions for the oxidation of hydrogen and CO on nickel and ceria anodes along with their kinetic parameters are given in tables 3 and 4, respectively. Diffusion flux of ceria surface species is arbitrarily considered as zero. Moreover, on the basis of experimental data and literature survey, the rate limitations were solely attributed to the charge transfer process compared to the defect transport in the bulk. So, while modeling ceria anodes, relevant mass transfer (reaction-diffusion) equations reduce to ordinary differential equations. Whereas, for nickel and YSZ surface species, coverage of each surface specie was calculated by solving coupled partial differential equations using Chebfun [39] function in Matlab software. Faradaic current was calculated from rate of charge transfer reactions leading to charge transfer resistance and hence the AC impedance.

Reaction mechanisms for the oxidation of hydrogen and CO on nickel are taken from [40] and [41, 42], respectively. Thermodynamic and kinetic parameters are also adopted from the same. The reaction mechanisms of hydrogen and CO

Physico-chemical process	Relevant equation	Eq. no
Rate of coverage of surface species	$\frac{\partial \theta_i}{\partial t}_{surf} = \frac{\sigma_i}{\Gamma_k}\dot{s}_i + \frac{\partial J_i^{surf}}{\partial x}_{surf}$	(7)
Diffusion flux	$J_i = -D_i \frac{\partial}{\partial x}\theta_i$	(8)
Specie production rate	$\dot{s}_i = \sum_m \nu_{i,m}\left(k_{f,m}\prod_r c_{i,r}^{\nu r} - k_{b,m}\prod_p c_{i,p}^{\nu p}\right)$	(9)
Forward reaction rate constant	$k_{f,m} = k_{f,m}^0 T^{\beta_m} exp\left(-\frac{E_m^{act}}{RT}\right)$	(10)
Backward reaction rate constant	$k_{b,m} = k_{f,m} exp\left(\frac{\Delta G_m}{RT}\right)$	(11)
Diffusion coefficient	$D^{surf} = D^0 exp\left(-\frac{E_{act}}{RT}\right)$	(12)
Faradaic current	$i_F = zFA_{CTRx}\left(k_{f,ct}\prod_r c_{i,r}^{\nu r} - k_{b,ct}\prod_p c_{i,p}^{\nu p}\right)$	(13)
Forward charge transfer rate constant	$k_{f,ct} = k_{f,ct}^0 exp\left(-\frac{E_{ct}^{act}}{RT}\right) exp\left(-\alpha\frac{zF}{RT}\eta\right)$	(14)
Backward charge transfer rate constant	$k_{r,ct} = k_{f,ct} exp\left(\frac{\Delta G_{ct}}{RT}\right)$	(15)
Voltage perturbation for EIS study	$\eta = V_0 sin(2\pi f t)$	(16)
Charge transfer resistance	$R_{ct} \approx \frac{d\eta}{di_F}$	(17)

Table 2: Summary of the relevant equations [40].

In above table, *i* refers to the bulk/surface species, *m* runs over all reactions involving surface/gas, surface/bulk and charge transfer reactions (*r* for reactant species, *p* for product species and *ct* for charge transfer).

oxidation on ceria anode are given in our previous article [31]. In the elementary kinetic model, the rate coefficients for the charge transfer reactions of individual hydrogen and CO oxidation were manually varied to obtain the best fit of experimental impedance spectra. Other parameters like capacitance values and CPE exponents were kept the same as obtained by ECM fitting. Thus fixing the parameters obtained by ECM fitting reduced the number of free fit parameters in kinetic modelling and focus could be asserted on the charge transfer process. For the simulation of syngas mixtures, all other parameters except gas phase concentrations were kept unchanged.

3. Experimental and modeling results

Previously [36], we briefly described the electrochemical oxidation of syngas (CO/H_2 mixtures) in dry gas environment. Results for the oxidation of hydrogen and CO as published previously [16] were also included for comparison. In this work, we extended the discussion including oxidation in wet gas environment as well to incorporate the effect of the WGS reaction on electrochemical oxidation.

3.1. Nickel pattern anodes

The intent of this study is to understand the electrochemical oxidation of different syngas compositions on nickel and ceria. Figure 4 shows the impedance spectra obtained with nickel pattern anodes at 800 ^oC and the activation energies for both high-frequency and low-frequency processes for different syngas compositions in the dry and wet gas environments.

Elementary Reaction	k_m^0 (or s_m^0)	E_m^{act} kJ.mol^{-1}
Ni surface reactions		
$H_2O_{gas} + o_{Ni} \rightleftharpoons H_2O_{Ni}$	1.4x10^{10} cm^3.mol^{-1}.s^{-1}	0
$H_{2gas} + 2o_{Ni} \rightleftharpoons 2H_{Ni}$	9.8x10^{17} cm^5.mol^{-2}.s^{-1}	0
$H_{Ni} + O_{Ni} \rightleftharpoons OH_{Ni} + o_{Ni}$	5.0x10^{22} cm^2.mol^{-1}.s^{-1}	97
$H_2O_{Ni} + O_{Ni} \rightleftharpoons 2OH_{Ni}$	5.4x10^{23} cm^2.mol^{-1}.s^{-1}	20.9
$OH_{Ni} + H_{Ni} \rightleftharpoons H_2O_{Ni} + o_{Ni}$	3.0x10^{20} cm^2.mol^{-1}.s^{-1}	43
$CO_{gas} + o_{Ni} \rightleftharpoons CO_{Ni}$	$s_m^0 = 0.5$	0
$CO_{gas} + O_{Ni} \rightleftharpoons CO_{2,gas} + o_{Ni}$	1.0x10^{23} cm^3.mol^{-1}.s^{-1}	181.8
$CO_{Ni} + O_{Ni} \rightleftharpoons CO_{2,Ni} + o_{Ni}$	2.0x10^{19} cm^2.mol^{-1}.s^{-1}	123.6
$CO_{2,Ni} \rightleftharpoons CO_{2,gas} + o_{Ni}$	7x10^{11} 1/s	41.0
YSZ surface reactions		
$H_2O_{gas} + o_{YSZ} \rightleftharpoons H_2O_{YSZ}$	6.6x10^{11} cm^3.mol^{-1}.s^{-1}	0
$O^{2-}_{YSZ} + H_2O_{YSZ} \rightleftharpoons 2OH_{YSZ}$	1.6x10^{22} cm^3.mol^{-1}.s^{-1}	9.6
$O^{2-}_{YSZ} + V_O^{\cdot\cdot} \rightleftharpoons O_O^x + o_{YSZ}$	1.6x10^{22} cm^3.mol^{-1}.s^{-1}	90.9
$CO_{gas} + o_{YSZ} \rightleftharpoons CO_{YSZ}$	$s_m^0 = 0.04$	
Charge transfer reactions		
$H_{Ni} + O^{2-}_{YSZ} \rightleftharpoons OH_{YSZ} + o_{YSZ} + e^-_{Ni}$	fit	134
$H_{Ni} + OH^-_{YSZ} \rightleftharpoons H_2O_{(g)} + o_{Ni} + o_{YSZ} + e^-_{Ni}$	fit	134
$O_O^x + o_{YSZ} \rightleftharpoons O^-_{YSZ} + V_O^{\cdot\cdot} + e^-_{Ni}$	fit	173
$CO_{Ni} + O^-_{YSZ} \rightleftharpoons CO_{2,gas} + o_{Ni} + o_{YSZ} + e^-_{Ni}$	fit	173

Table 3: Elementary reactions for hydrogen and CO oxidation on nickel pattern anodes [40, 41].
In the above table, o_{Ni} is a free adsorption site at nickel surface, o_{YSZ} a free adsorption site at YSZ surface, O_O^x lattice oxygen in YSZ, $V_O^{\cdot\cdot}$ oxide ion vacancy with an effective charge +2, O^{2-}_{YSZ} oxide ion at YSZ surface, e^-_{Ni} electron in the nickel, and all other species indicate adsorbed species at nickel surface with Ni subscript and YSZ surface species with YSZ subscript.

Elementary Reaction	k_m^0	E_m^{act} kJ.mol^{-1}
$H_{2,gas} + 2o_{ce} \rightleftharpoons 2H_{ads}$	8x10^{10} cm^5.mol^{-2}.s^{-1}	131.0
$H_{ads} + O^{2-}_{ce} \rightleftharpoons OH^-_{ads} + o_{ce} + e^-$	fit	133.0
$H_{ads} + OH^-_{ads} \rightleftharpoons H_2O_{gas} + 2\,o_{ce} + e^-$	fit	133.0
$CO_{gas} + 2O_O^x \rightleftharpoons CO_3^x$	3x10^{13} cm^5.mol^{-2}.s^{-1}	212.0
$CO_3^x \rightleftharpoons CO_{2,gas} + O_O + V_O^{\cdot\cdot} + 2e^-_t$	fit	117.0

Table 4: Elementary reactions for hydrogen and CO oxidation on Ceria pattern anodes [31].
In the above table, o_{ce} is a free adsorption site at ceria surface, O^{2-}_{ce} oxide ion at ceria surface, O_O^x lattice oxygen, and $V_O^{\cdot\cdot}$ is the oxide ion vacancy.

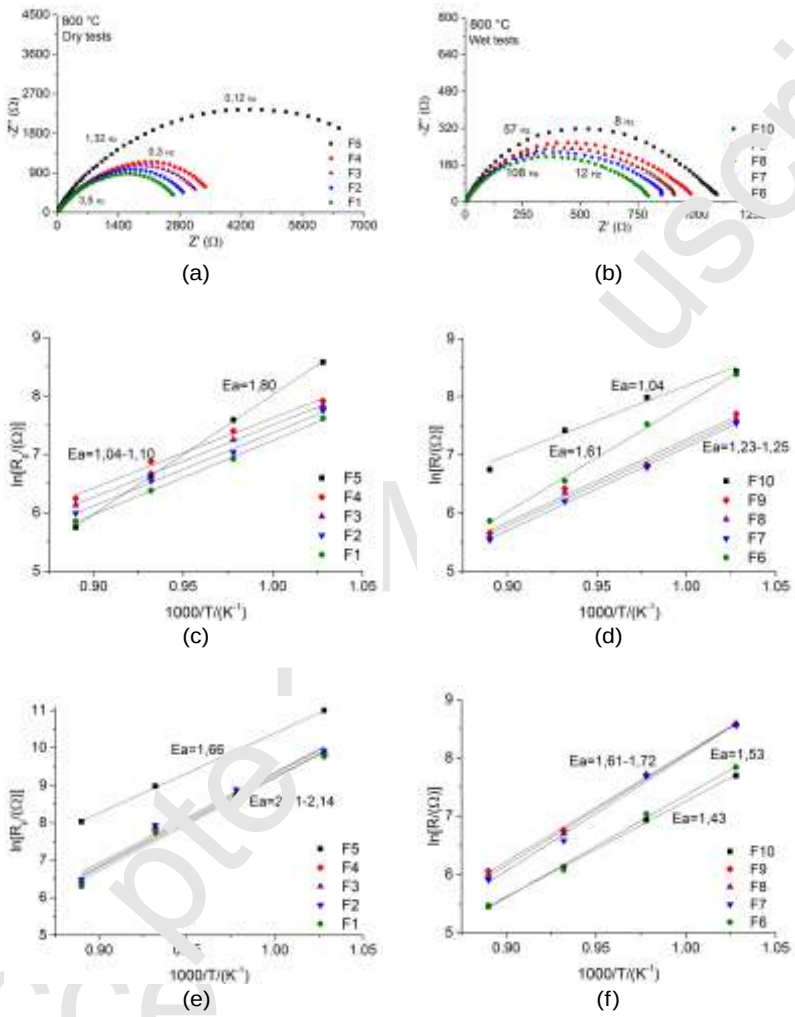

Figure 4: Electrochemical oxidation of syngas on nickel pattern anodes; Impedance spectra at 800 ^{o}C (a), Arrhenius plot for high-frequency (c) and low-frequency (e) process in dry gas environment. Impedance spectra at 800 ^{o}C (b), Arrhenius plot for high-frequency (d) and low-frequency (f) process in wet gas environment. Activation energies are given in eV.

Parameter	Gas atmosphere		
	H_2/H_2O	CO/CO_2	CO/H_2O
Q_1	$6.2x10^{-3}$	$2.0x10^{-4}$	$5.6x10^{-4}$
Q_2	$6.4x10^{-4}$	$2.1x10^{-4}$	$3.7x10^{-4}$
n_1	0.67	0.7	0.77
n_2	0.60	0.66	0.70

Table 5: Equivalent circuit fitting parameters for H_2/H_2O (F6), CO/CO_2 (F5), and CO/H_2O (F10) on nickel pattern anodes.

3.1.1. Oxidation in dry environment

Figure 4 (a) shows that the polarization resistance for oxidation of CO (F5) is almost 2.5 times higher than that of hydrogen (F1). Higher polarization resistance and lower cell performance with CO compared to hydrogen on nickel anodes are reported [5, 9, 43, 16, 44, 29]. With the addition of small amounts of hydrogen to the CO gas stream, the polarization resistance drops drastically. Sudden drop in polarization resistance is attributed to hydrogen preferential oxidation, here termed as "H_2-PROX". Further increase in hydrogen fraction results only in the gradual decrease of the polarization resistance. Effect of hydrogen oxidation kinetics is so significant that the impedance spectra for all CO/H_2 gas mixtures (F2-F4) is much closer to hydrogen (F1) than CO (F5). This refers to the possibility that hydrogen is electrochemically oxidized while CO mainly acts as a diluent [16].

Impedance spectra are also fitted to the equivalent circuit model (ECM) as shown in figure 3. The fitting parameters for three gas environments are shown in table 5. Figure 4 (c and e) shows the temperature dependence of high-frequency and low-frequency processes obtained from ECM fitting. The activation energies of both high-frequency and low-frequency processes for the oxidation of hydrogen and CO/H_2 mixtures are almost the same and agrees well with the argument of H_2-PROX. In CO/CO_2 environment, the high-frequency process is found to be highly thermally activated (Ea = 1.80 eV) and attributed to the electrochemical/charge transfer process. This charge transfer process may be either oxygen spillover from YSZ to the nickel or direct involvement of gaseous CO in the charge transfer step [16]. Low-frequency activation energy is also relatively high (Ea = 1.66 eV), that makes difficult to identify a rate-limiting process. Possible rate-limiting processes are discussed elsewhere [16, 45].

3.1.2. Oxidation in wet environment

Figure 4 (b, d and f) shows impedance spectra and activation energies in the wet gas environment (4 % moisture). It is noticed that the polarization resistance for wet hydrogen oxidation (F6) is only one fourth of the resistance observed in case of dry hydrogen oxidation (F1) at 800 ^oC. Similarly, the

polarization resistance of wet CO oxidation (F10) is less than one sixth of the resistance observed in case of dry CO oxidation (F5). Relaxation frequency (f_s) for both low and high-frequency processes also increases by more than an

order of magnitude. This indicates that adding water to hydrogen and CO feed gas strongly stimulates the oxidation process. The accelerating effect of water addition on hydrogen oxidation process is documented [46, 47, 48]. While the effect on CO oxidation is possibly related to heterogeneous WGS conversion and subsequent preferential oxidation of hydrogen. Unlike dry gas environment, adding hydrogen to wet CO does not lead to a drastic decrease in the polarization resistance. Rather, the polarization resistance gradually decreases from wet CO (F10) to wet hydrogen (F6).

Activation energies of high-frequency and low-frequency processes for hydrogen oxidation are 1.61 and 1.43 eV, respectively. It is clear that the high-frequency process is highly thermally activated which usually points towards an electrochemical charge transfer like process. High-frequency activation energies for CO/H_2 mixtures lie between the values obtained for wet hydrogen and wet CO gas environments. The effect of increasing steam partial pressure in CO gas feed stream on the polarization resistance and relaxation frequency is shown in figure 5. It is clear that with increase in steam partial pressure, polarization resistance decreases and the relaxation frequency increases for both high-frequency and low-frequency process.

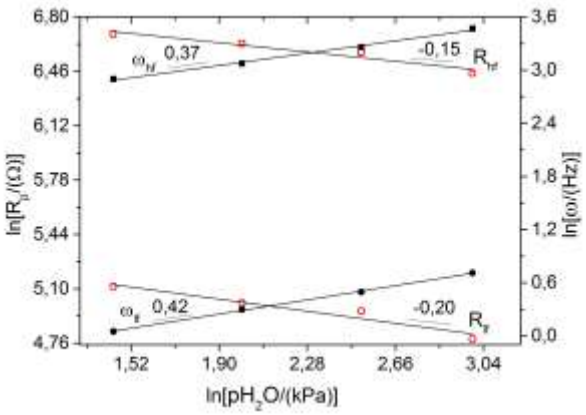

Figure 5: Effect of steam partial pressure on polarization resistance and relaxation frequency of high-frequency (hf) and low-frequency (lf) processes at 800 °C

3.1.3. Modeling results

Figure 6 shows experimental and simulated impedance spectra for H_2/H_2O, CO/CO_2 and wet CO environments. Kinetic parameters obtained by model fitting of H_2/H_2O and CO/CO_2 systems are used for simulating wet CO and CO/H_2 environments. Mass balance equations of surface species on both nickel and YSZ are solved simultaneously. The capacitance and exponent values for high frequency and low frequency processes are shown in table 5. The results indicate a reasonably good qualitative agreement between experimental and simulated spectra for H_2/H_2O and CO/CO_2 environments and slightly over-predicts the polarization resistance for wet CO environment. The misalignment between experimental and simulated peaks for wet CO is apparent on Bode plots (figure 6 b): the simulations predict that the peak occurs at lower frequencies than the observed ones. Further optimization of the model for co-oxidation may address this discrepancy. The simulated rate of charge transfer reactions for hydrogen and CO oxidation in wet CO environment (F10) are found to be 6.9×10^{-11} and 1.2×10^{-11} mol.cm^{-2}.s^{-1}, respectively. Clearly the rate of charge transfer reaction for hydrogen oxidation is higher than CO despite of very low concentration of hydrogen.

Figure 7 compares the impedance spectra resulting from all three current calculation scenarios: a) from hydrogen oxidation only b) from CO oxidation only and c) if both hydrogen and CO contribute to total faradaic current. It can be seen that the impedance spectra simulated by considering only hydrogen oxidation ($i_F = i_{H_2}$) is closer to the experimental spectra than considering CO oxidation ($i_F = i_{CO}$) alone. This indicates that during oxidation of wet CO, a larger fraction of current is produced from hydrogen oxidation. This is inline with the argument of hydrogen preferential oxidation. Considering co-oxidation ($i_F = i_{H_2} + i_{CO}$), a slightly better match to experimental spectra is found which created an interest to quantify the current fraction produced from hydrogen oxidation.

Hydrogen current fraction is defined as the ratio of current produced by hydrogen oxidation to the total current produced by hydrogen and CO co-oxidation. Hydrogen current fraction as a function of hydrogen fraction in the syngas is shown in figure 8. It is found that at a very low hydrogen concentration (5 %), almost 85 % current is solely produced by hydrogen oxidation. While remaining 15 % current is obtained from CO oxidation. That is why, best match to experimental data in figure 7 is obtained from co-oxidation. With increase in hydrogen fraction, hydrogen current fraction also increases. For example, at equimolar hydrogen and CO concentration, hydrogen current fraction is almost 0.97 which indicates that direct CO oxidation is negligible.

3.2. Ceria pattern anodes

The electrochemical impedance spectra and the activation energies for both dry and wet gas environments are shown in figure 9 (a) and (b), respectively.

EIS of ceria has shown two clearly distinct arcs, i.e., a relatively small and depressed arc at high-frequency end (shown in the inserts) and the main impedance

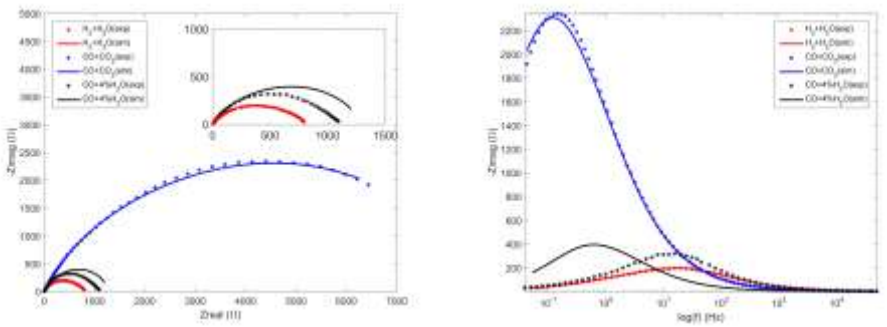

(a) (b)

Figure 6: Model fitting and experimental data on nickel anodes for H_2 /H_2O, CO/CO_2 and wet CO (4 % H_2O systems a) Nyquist plots b) Bode plots. exp indicates experimental and sim indicates simulated data.

Parameter	dry H_2	dry CO	wet H_2	wet CO
E_a [eV]	0.80	0.89	0.75	0.85
f_s [kHz] @800^{o}C	6.92	5.48	20.52	7.86
C_{eq} [μF.cm^{-2}] @800^{o}C	5.30	1.31	1.14	9.11

Table 6: Typical characteristics of high-frequency arc

arc at low-frequency end. The polarization resistance of high-frequency arc is significantly lower than the low-frequency arc and thus not considered to be the rate-limiting. Main characteristics of high-frequency arc at 800^{o}C are shown in table 6. It is found that the gas environment has not a considerable influence on the polarization resistance and activation energy of high-frequency process. Model fitting at different temperatures further revealed that the capacitance is mainly independent of temperature. Both of these observations suggest that the high-frequency process can not be related to a charge transfer process. Similar arcs at high-frequency end were also observed in other studies and associated to a grain boundary effect [49, 50] and poor contact between electrode and the current collector [51]. The capacitance implied for the low-frequency arc is on the order of 10^{-3}-10^{-4} F.cm^{-2} which is characteristic of the gas/solid interface [52]. Hence, the resistance associated to the low-frequency arc is attributed to the electrochemical process at gas/ceria interface and discussed here in detail.

3.2.1. Oxidation in dry environment

Impedance spectroscopy reveals that the polarization resistance with ceria is much lower than nickel for all gas environments tested here. Previously this observation was related to a larger electrochemically active region on ceria compared with nickel [23]. Figure 9a shows that the polarization resistance for CO oxidation (F5) is almost five times higher than for hydrogen (F1).

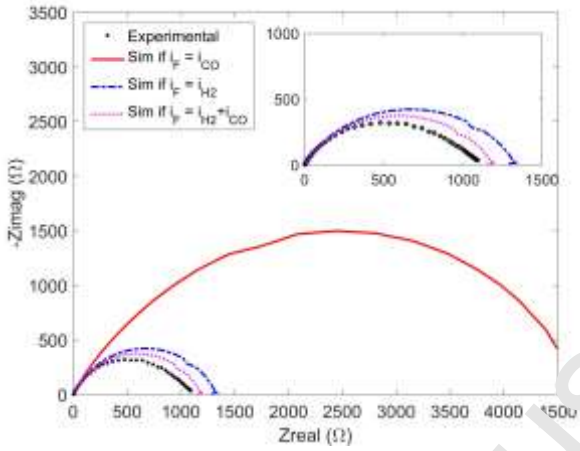

Figure 7: Electrochemical impedance of nickel anodes if faradaic current is a result of hydrogen (i_{H_2}), CO (i_{CO}) and H_2+CO ($i_{H_2} + i_{CO}$) oxidation. Experimental data is also shown for comparison.

Whereas, this difference is only 2.5 times in case of nickel anodes (figure 4a, F5 vs F1). Surface characterization techniques like XPS and IR have shown the formation of intermediate carbonate species on ceria surface when exposed to CO [34, 53]. Decomposition of these intermediates to produce gas phase CO_2 is highly energy demanding. Thus, very high polarization resistance for CO relative to hydrogen may be attributed to high surface coverage of carbonate species with decomposition/desorption step as the rate determining [54, 31].

Adding a small amount of hydrogen to the CO feed (F4), drops polarization resistance drastically indicating H_2-PROX. Further increase in hydrogen fraction does not lead to a substantial drop in the polarization resistance. Effect of hydrogen oxidation kinetics is so significant that the size of impedance spectra for all syngas mixtures (F2-F4) is much closer to the hydrogen (F1) than to the CO (F5). Low-frequency activation energies for syngas oxidation (figure 9e) are also similar to that of hydrogen oxidation. It is, therefore, speculated that in syngas hydrogen preferentially oxidizes while CO mainly forms surface carbonates and inhibits hydrogen adsorption and subsequent oxidation. Possible reaction mechanism and the rate-limiting processes for electrochemical oxidation of hydrogen and CO are detailed elsewhere [16, 31].

3.2.2. Oxidation in wet environment

Impedance spectra of hydrogen, CO and syngas oxidation in wet environment are shown in figure 9b. When compared with dry environment (figure 9a), it is noticed that the polarization resistance for wet hydrogen oxidation (F6) is only one fifth of the resistance observed in case of dry hydrogen oxidation (F1). Similarly, the polarization resistance of wet CO oxidation (F10) is less than one tenth of the resistance observed for dry CO oxidation (F5). Interestingly, the

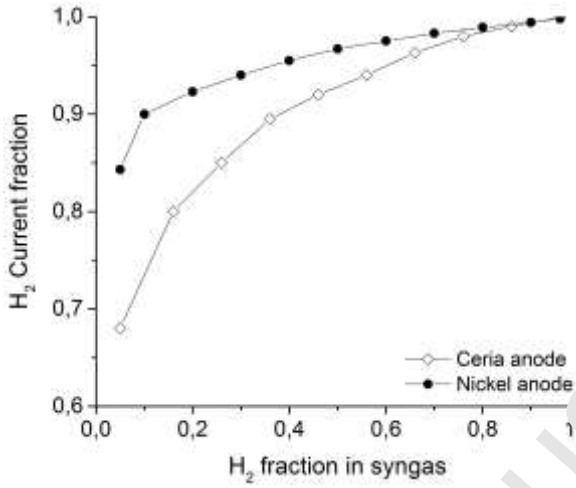

Figure 8: Effect of hydrogen fraction in syngas on hydrogen current fraction at 800 ^{o}C

polarization resistance for CO (F10) is still almost twice of the hydrogen (F6). Whereas, polarization resistance for hydrogen oxidation on nickel was only 40 percent higher than that of CO oxidation. Relatively higher resistance of CO oxidation on ceria may be related to the formation of carbonates. Low-frequency and high-frequency activation energies for wet environment are shown in figure 9d and 9f, respectively. It is found that the low-frequency activation energy for CO oxidation is the same in both dry and wet gas environment. This suggests that adding water to CO does not affect the rate limitations. Conversely, adding water to hydrogen (F6) and syngas mixtures (F7-F9) drops the activation barrier significantly. As surface chemistry and the charge transfer processes are lumped together in the main arc, so it is difficult to separate and quantify the effect of steam addition on individual process. The effect of varying steam partial pressure on wet CO electrochemistry is shown in figure 10. It can be seen that the polarization resistance decreases when the amount of water in the fuel gas is increased. This is inline with the observation made in case of nickel anode (figure 5). However, the slope of ln[pH_2O] vs ln[Rp] curve for ceria is found to be -0.10 which in case of nickel anode was -0.15. This observation probably suggests that the addition of water has more accelerating effect on the overall CO oxidation process on nickel anodes compared with the ceria anodes.

3.2.3. Modeling results

Elementary reactions for hydrogen and CO oxidation on ceria are given in table 4. Model fitting and experimental data for all three gas environments (H_2 /H_2O, CO/CO_2 and wet CO) are shown in fig 11. Rate of charge transfer reactions for hydrogen and CO oxidation in wet CO environment are found to be 10.0x10^{-11} and 5.5x10^{-11} mol.cm^{-2}.s^{-2}, respectively. Interestingly, the rate of hydrogen oxidation in wet CO environment is only twice of the rate of

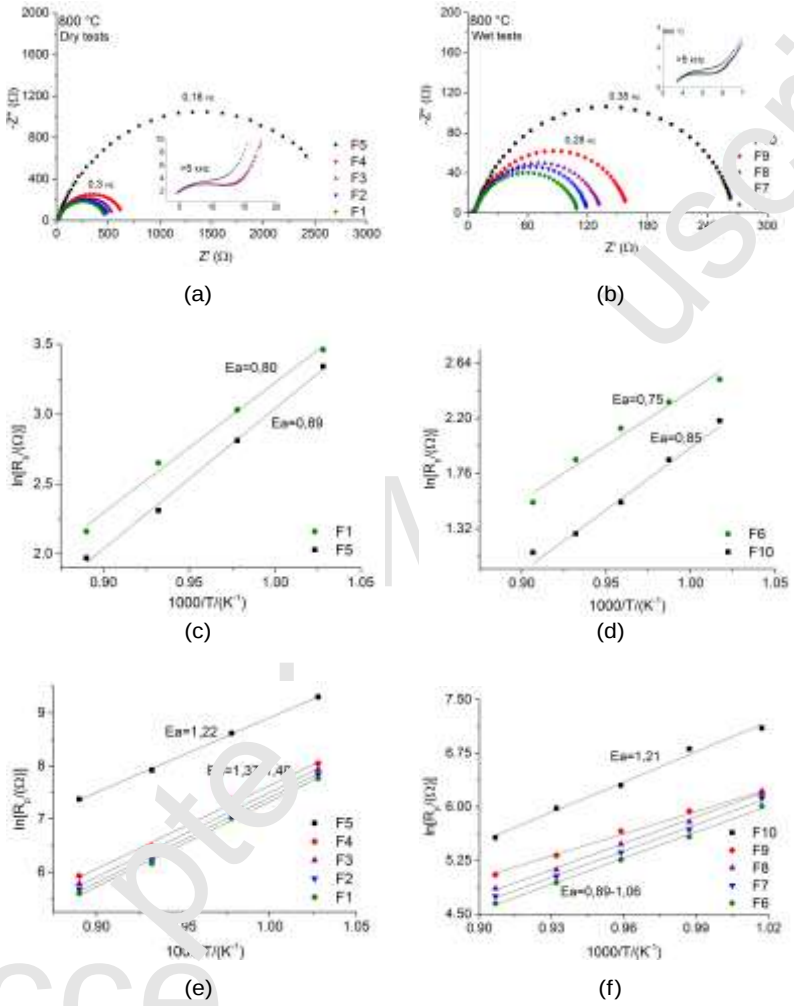

Figure 9: Electrochemical oxidation of syngas on ceria pattern anodes; Impedance spectra at 800 °C (a), Arrhenius plot for high-frequency (c) and low-frequency (e) process in dry gas environment. Impedance spectra at 800 °C (b), Arrhenius plot for high-frequency (d) and low-frequency (f) process in wet gas environment. Activation energies are given in eV.

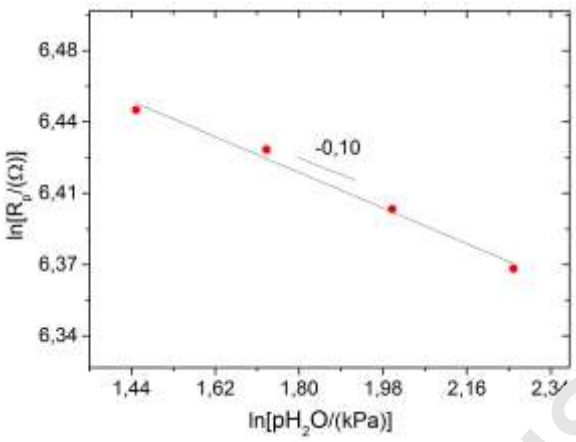

Figure 10: Effect of steam partial pressure on low-frequency polarization resistance at 780 ^{o}C

CO oxidation. Figure 12 compares the impedance spectra resulting from all three current calculation scenarios as explained in section 3.1.3. It can be seen that neither current obtained from CO oxidation ($i_F = i_{CO}$) nor from hydrogen oxidation ($i_F = i_{H_2}$) matches the experimental spectra. Rather co-oxidation of hydrogen and CO ($i_F = i_{H_2} + i_{CO}$) gives best qualitative representation of the experimental spectra. Similar to the nickel anode, a misalignment between experimental and simulated peaks is also apparent for wet CO (figure 11 b). Relative contribution of hydrogen and CO oxidation in syngas is simulated as shown in figure 8. It is found that though hydrogen current fraction is higher than CO, yet it is much lower than the fraction found in the case of nickel anode. For 5 % hydrogen in the feed, only 68 % current is produced from hydrogen oxidation. At equimolar concentrations, almost 93 % current is obtained from hydrogen oxidation and remaining 7 % from CO. This indicates that while studying syngas oxidation of ceria, electrochemical oxidation of CO can not be ignored.

3.3. Comparison between nickel and ceria anodes

Based on the results discussed in previous sections, nickel and ceria anodes are compared with respect to 1) cell performance in hydrogen and CO 2) hydrogen preferential oxidation in syngas, and 3) effect of hydrogen concentration on hydrogen current fraction.

Polarization resistance for oxidation of hydrogen (F1), CO (F5), and CO/H_2 mixture (F4) in dry environment are compared in table 7. Better cell performance with hydrogen than CO on nickel is inline with the literature [5, 9, 16, 29, 44, 43]. However, the cell performance with hydrogen and CO on ceria is contradictory to the reported trend [29]. In [29], it is observed that the cell performance with Cu/CeO_2/YSZ anode is identical when using either hydrogen or CO while we found very high polarization resistance for CO in comparison to hydrogen. It

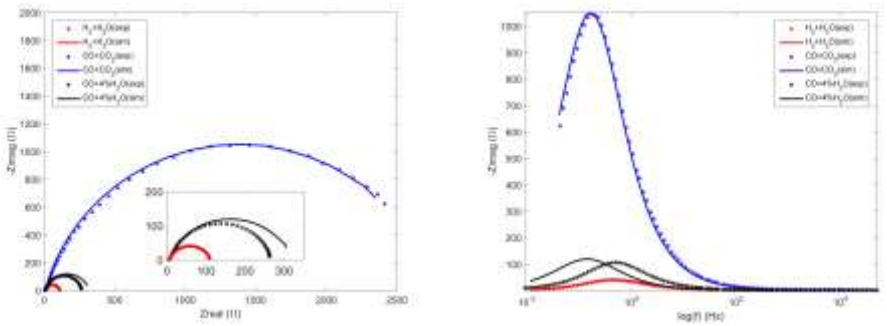

(a) (b)

Figure 11: Model fitting and experimental data on ceria anodes for H_2 /H_2O, CO/CO_2 and wet CO (4 % H_2O systems a) Nyquist plots b) Bode plots.

Fuel no.	Polarization resistance (Ω)	
	nickel	ceria
F1 (H_2)	2890	480
F4 (CO/H_2)	3860	670
F5 (CO)	8600	2750

Table 7: Polarization resistance for hydrogen (F1), CO (F5) and CO/H_2 mixture (F4) oxidation on nickel and ceria anodes

is worthwhile remembering that, oxidation on both pure ceria and Cu/CeO_2 is expected to take place only on the ceria phase [30]. Thus, further investigations are suggested.

In case of CO/H_2 mixture, the polarization resistance is closer to that of hydrogen compared to CO. This clearly indicates that the oxidation process of mixtures resembles to hydrogen oxidation instead of CO, which we regard as hydrogen preferential oxidation. This effect is observed on both nickel and ceria anodes. Using nickel anodes, better cell performance with CO/H_2 mixtures than CO is reported as discussed in section 1. However, using ceria anodes, such studies are not known to our knowledge besides preliminary results presented in our previous work [16].

Electrochemical co-oxidation of hydrogen and CO is studied by elementary kinetic modeling. In wet CO (F6), rate of charge transfer reactions for CO is almost one sixth of the hydrogen on nickel and only half of the hydrogen on ceria. These reaction rates correspond to hydrogen current fraction of 0.85 and 0.65 for nickel and ceria, respectively. Then hydrogen current fraction is further evaluated for a wide range of hydrogen fractions in the syngas (figure 8). It is found that increasing hydrogen fraction in syngas, hydrogen current fraction also increases for both nickel and ceria. For example, hydrogen current fraction in equimolar mixture is 0.97 for nickel and 0.93 for ceria. Thus, in equimolar

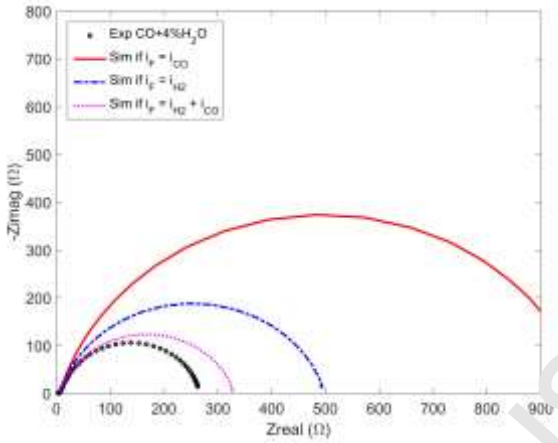

Figure 12: Electrochemical impedance of ceria anodes if faradaic current is a result of hydrogen (i_{H_2}), CO (i_{CO}) and H_2+CO ($i_{H_2} + i_{CO}$) oxidation. Experimental data is also shown for comparison.

mixture, 3 % and 7 % current is expected from CO oxidation on nickel and ceria anodes, respectively.

4. Conclusions:

In this study, electrochemical oxidation of hydrogen, CO and syngas (CO/H_2 mixtures) on nickel and ceria pattern anodes was investigated. Experimental results from impedance spectroscopy were presented for both dry and wet gas environment. Further, elementary kinetic model was developed to understand hydrogen and CO co-oxidation. The main results are summarized as;

- The polarization resistance for hydrogen oxidation is less than CO oxidation for both nickel and ceria anodes. The polarization resistance for syngas oxidation is closer to that of hydrogen oxidation than CO. Moreover, the activation energies (obtained by equivalent circuit model fitting) for syngas are similar to that of hydrogen oxidation. This suggests that the oxidation of syngas resembles hydrogen oxidation and hydrogen is preferentially oxidized.

- Addition of water to CO leads to a significantly larger drop in the polarization resistance than the drop caused by the addition of water to hydrogen. However, the polarization resistance for CO/H_2 mixture was still higher than H_2/H_2O mixture. Larger drop in the polarization resistance in former case is attributed to the combined effect of water gas shift conversion and preferential oxidation of hydrogen produced via CO conversion. Preferential oxidation of hydrogen produced via water-gas-shift conversion was also captured by kinetic model.

- Majority of the membrane-electrode-assembly (MEA) models neglect CO electrochemistry in CO/H_2 mixtures assuming that hydrogen is the only electrochemically active specie while CO undergoes water-gas-shift transformation. In this study, simulation has shown that CO may also electrochemically oxidize depending upon its concentration in the syngas. For example, at equimolar hydrogen/CO concentration, 3 % of the total current was obtained from CO oxidation in case of nickel and 7 % in case of ceria anode. For confirming and better understanding of relatively larger contribution of CO electrochemistry in case of ceria than nickel anode, further investigations are required.

Limited knowledge of the reaction mechanisms and rate-limiting step(s) was found for hydrogen and CO electrochemical oxidation on ceria that will be addressed in future studies. Also, the effect of current density on hydrogen and CO co-oxidation will be focused. This will help in better understanding of the oxidation process and lead to the development of kinetic equations based on the rate-limiting-step(s). Such kinetic equations may be used in the macro-level models instead of the empirical relations for the prediction of fuel cell performance. Future work will also concentrate on extending these kinetics to a macro-level simulation of real syngas environments including various contaminants. The generated knowledge is expected to contribute to the selection/design of suitable cells for specific fuels.

Acknowledgment

This work has been supported by the University of Engineering and Technology Lahore (UET), Pakistan through a PhD fellowship under Faculty Development Program (FDP). We are thankful to UET for funding this work. We also gratefully acknowledge Prof. Joop Schoonman for useful comments on this manuscript.

List of symbols:

Symbol	Unit	Description
c	$mol.cm^{-3}$	area specific concentrations $c_i = \Gamma_k \theta_i$ for surface & $c_i = \frac{P_i}{RuT}$ gas species
C_{eq}	F	capacitance
D_i^{surf}	$cm^2.s^{-1}$	surface diffusion coefficient of specie i
D_i^0	$cm^2.s^{-1}$	tracer diffusion coefficient of specie i
E^{act}	$J.mol^{-1}$	activation energy
f_s	Hz	relaxation frequency
F	$C.mol^{-1}$	Faraday constant (96485 $C.mol^{-1}$)
ΔG	$J.mol^{-1}$	Gibbs free energy
i_F	A	faradaic current
k_f&k_b	–	forward and backward reaction rate constants respectively
R	$J.mol^{-1}.K^{-1}$	universal gas constant (8.314 $J.mol^{-1}.K^{-1}$)
R_p,R_1& R_2	ohm	Polarization resistances
R_{ct}	ohm	charge transfer resistance
$\dot{s}$	$mol.cm^{-2}.s^{-1}$	species production rate
T	K	temperature
V_o	V	amplitude of voltage perturbation
x	cm	spatial dimension perpendicular to the TPB line
Q	Fs^{n-1}	parameter of constant phase element
z	–	number of electrons involved in charge transfer reaction
Z	ohm	impedance
Greek		
α	–	transfer coefficient
β	–	temperature coefficient
η	V	sinusoidal voltage perturbation
θ		dimensionless surface coverage
Γ	$mol.cm^{-2}$	area specific surface site density
σ	–	number of surface sites occupied by surface specie

References

[1] S. C. Singhal, K. Kendall, High-temperature solid oxide fuel cells: fundamentals, design and applications: fundamentals, design and applications, Elsevier, 2003.

[2] R. J. Kee, H. Zhu, A. M. Sukeshini, G. S. Jackson, Solid Oxide Fuel Cells: operating principles, current challenges, and the role of syngas, Combust. Sci. Technol. 180 (2008) 1207–1244.

[3] D. Papurello, A. Lanzini, L. Tognana, S. Silvestri, M. Santarelli, Waste to energy: exploitation of biogas from organic waste in a 500 W el solid oxide fuel cell (SOFC) stack, Energy 85 (2015) 145–158.

[4] V. Chiodo, A. Galvagno, A. Lanzini, D. Papurello, F. Urbani, M. Santarelli, S. Freni, Biogas reforming process investigation for SOFC application, Energy Conversion and Management 98 (2015) 252–258.

[5] Y. Matsuzaki, I. Yasuda, Electrochemical oxidation of H_2 and CO in a H_2-H_2O-CO-CO_2 system at the interface of a Ni-YSZ cermet electrode and YSZ electrolyte, J. Electrochem. Soc. 147 (2000) 1630–1635.

[6] Y. Jiang, A. V. Virkar, Fuel composition and diluent effect on gas transport and performance of anode-supported SOFCs, J. Electrochem. Soc. 150 (2003) A942–A951.

[7] A. Weber, B. Sauer, A. C. Müller, D. Herbstritt, E. Ivers-Tiffée, Oxidation of H_2, CO and methane in SOFCs with Ni/YSZ-cermet anodes, Solid State Ionics 152 (2002) 543–550.

[8] K. Sasaki, Y. Hori, R. Kikuchi, K. Eguchi, A. Ueno, H. Takeuchi, M. Aizawa, K. Tsujimoto, H. Tajiri, H. Nishikawa, et al., Current-voltage characteristics and impedance analysis of Solid Oxide Fuel Cells for mixed H_2 and CO gases, J. Electrochem. Soc. 149 (2002) A227–A233.

[9] A. M. Sukeshini, B. Habibzadeh, B. P. Becker, C. A. Stoltz, B. W. Eichhorn, G. S. Jackson, Electrochemical oxidation of H_2, CO, and CO/H_2 mixtures on patterned Ni anodes on YSZ electrolytes, J. Electrochem. Soc. 153 (2006) A705–A715.

[10] R. Suwanwarangkul, E. Croiset, E. Entchev, S. Charojrochkul, M. Pritzker, M. Fowler, P. Douglas, S. Chewathanakup, H. Mahaudom, Experimental and modeling study of Solid Oxide Fuel Cell operating with syngas fuel, J. Power Sources 161 (2006) 308–322.

[11] C. Bao, X. Zhang, One-dimensional macroscopic model of Solid Oxide Fuel Cell anode with analytical modeling of H_2/CO electrochemical co-oxidation, Electrochim. Acta 134 (2014) 426–434.

[12] M. Andersson, J. Yuan, B. Sundén, Sofc modeling considering hydrogen and carbon monoxide as electrochemical reactants, J. Power Sources 232 (2013) 42–54.

[13] M. Ni, Modeling of sofc running on partially pre-reformed gas mixture, Int. J. Hydrogen Energy 37 (2012) 1731–1745.

[14] C. J. Moyer, N. P. Sullivan, H. Zhu, R. J. Kee, Polarization characteristics and chemistry in reversible tubular solid-oxide cells operating on mixtures of H_2, CO, H_2O, and CO_2, J. Electrochem. Soc. 158 (2011) B117–B131.

[15] K. M. Ong, Modeling of solid oxide fuel cell performance with coal gasification, Ph.D. thesis, Massachusetts Institute of Technology, 2016.

[16] H. Patel, A. Tabish, F. Comelli, P. Aravind, Oxidation of H_2, CO and syngas mixtures on ceria and nickel pattern anodes, Appl. Energy 154 (2015) 912–920.

[17] C. Bao, Z. Jiang, X. Zhang, Mathematical modeling of synthesis gas fueled electrochemistry and transport including H_2/CO co-oxidation and surface diffusion in Solid Oxide Fuel Cell, J. Power Sources 294 (2015) 317–332.

[18] A. Faes, A. Hessler-Wyser, A. Zryd, et al., A review of redox cycling of Solid Oxide Fuel Cells anode, Membranes 2 (2012) 585–664.

[19] H. Miao, G. Liu, T. Chen, C. He, J. Peng, S. Ye, W. G. Wang, Behavior of anode-supported SOFCs under simulated syngases, J. Solid State Electrochem. 19 (2015) 639–646.

[20] M. Mogensen, N. M. Sammes, G. A. Tompsett, Physical, chemical and electrochemical properties of pure and doped ceria, Solid State Ionics 129 (2000) 63–94.

[21] J.-S. Kim, V. V. Nair, J. M. Vohs, R. J. Gorte, A study of the methane tolerance of LSCM-YSZ composite anodes with Pt, Ni, Pd and ceria catalysts, Scripta Materialia 65 (2011) 90–95.

[22] A. Trovarelli, P. Fornasiero, Catalysis by ceria and related materials, volume 2, Imperial College Press London, 2002.

[23] H. Patel, N. Biradar, V. Venkataraman, P. Aravind, Ceria electrocatalysis compared to Nickel using pattern anodes, Int. J. Electrochem. Sci 9 (2014) 4048–4053.

[24] S. Hilaire, X. Wang, T. Luo, R. Gorte, J. Wagner, A comparative study of water-gas-shift reaction over ceria supported metallic catalysts, Appl. Catal., A 215 (2001) 271–278.

[25] J. Rodriguez, S. Ma, P. Liu, J. Hrbek, J. Evans, M. Perez, Activity of CeOx and TiOx nanoparticles grown on Au(111) in the water-gas-shift reaction, Science 318 (2007) 1757–1760.

[26] S. C. DeCaluwe, Quantifying the role of cerium oxide as a catalyst in solid oxide fuel cell, Ph.D. thesis, University of Maryland, 2009.

[27] P. Aravind, J. Ouweltjes, N. Woudstra, G. Rietveld, Impact of biomass-derived contaminants on sofcs with Ni/Gadolinia-doped ceria anodes, Electrochem. Solid-State Lett. 11 (2008) B24–B28.

[28] R. Gorte, J. Vohs, Nanostructured anodes for Solid Oxide Fuel Cells, Current Opinion in Colloid & Interface Science 14 (2009) 236–244.

[29] O. Costa-Nunes, R. J. Gorte, J. M. Vohs, Comparison of the performance of Cu-CeO_2-YSZ and Ni-YSZ composite sofc anodes with H_2, CO, and syngas, J. Power Sources 141 (2005) 241–249.

[30] C. Lu, W. Worrell, J. Vohs, R. Gorte, A comparison of Cu-ceria-SDC and Au-ceria-SDC composites for SOFC anodes, J. Electrochem. Soc. 150 (2003) A1357–A1359.

[31] H. Patel, A. Tabish, P. Aravind, Modelling of elementary kinetics of H_2 and CO oxidation on ceria pattern cells, Electrochim. Acta (2015).

[32] A. Donazzi, M. Rahmanipour, M. Maestri, G. Groppi, L. Bardini, A. Pappacena, M. Boaro, Experimental and model analysis of the co-oxidative behavior of syngas feed in an intermediate temperature solid oxide fuel cell, J. Power Sources 306 (2016) 467–480.

[33] C. Zhang, Y. Yu, M. E. Grass, C. Dejoie, W. Ding, K. Gaskell, N. Jabeen, Y. P. Hong, A. Shavorskiy, H. Bluhm, et al., Mechanistic studies of water electrolysis and hydrogen electro-oxidation on high temperature ceria-based solid oxide electrochemical cells, J. Am. Chem. Soc. 135 (2013) 11572–11579.

[34] Y. Yu, B. Mao, A. Geller, R. Chang, K. Gaskell, Z. Liu, B. W. Eichhorn, CO_2 activation and carbonate intermediates: an operando AP-XPS study of CO_2 electrolysis reactions on solid oxide electrochemical cells, Phys. Chem. Chem. Phys. 16 (2014) 11633–11639.

[35] P. Aravind, J. Ouweltjes, J. Schoonman, Diffusion impedance on nickel/gadolinia-doped ceria anodes for Solid Oxide Fuel Cells, J. Electrochem. Soc. 156 (2009) B1417–B1422.

[36] A. N. Tabish, H. C. Patel, F. Comelli, P. Aravind, Electrochemical oxidation of CO/H_2 mixtures on Ni and Ceria pattern anodes, in: ECS Conference on Electrochemical Energy Conversion & Storage with SOFC-XIV (July 26-31, 2015), ECS, 2015.

[37] H. Patel, V. Venkataraman, P. Aravind, Nickel pattern anodes for studying sofc electrochemistry, Advances in Solid Oxide Fuel Cells IX: Ceramic Engineering and Science Proceedings, Volume 34 (2013) 89.

[38] D. Papurello, A. Lanzini, D. Drago, P. Leone, M. Santarelli, Limiting factors for planar Solid Oxide Fuel Cells under different trace compound concentrations, Energy 95 (2016) 67–78.

[39] T. A. Driscoll, N. Hale, L. N. Trefethen (Eds.), Chebfun Guide, Pafnuty Publications Oxford, 2014. URL: http://www.chebfun.org/.

[40] M. Vogler, A. Bieberle-Hütter, L. Gauckler, J. Warnatz, W. G. Bessler, Modelling study of surface reactions, diffusion, and spillover at a Ni/YSZ patterned anode, J. Electrochem. Soc. 156 (2009) B663–B672.

[41] V. Yurkiv, A. Utz, A. Weber, E. Ivers-Tiffée, H.-R. Volpp, W. G. Bessler, Elementary kinetic modeling and experimental validation of electrochemical CO oxidation on Ni/YSZ pattern anodes, Electrochim. Acta 59 (2012) 573–580.

[42] J. Hanna, W. Lee, A. Ghoniem, Kinetics of carbon monoxide electro-oxidation in Solid Oxide Fuel Cells from Ni-YSZ patterned-anode measurements, J. Electrochem. Soc. 160 (2013) F698–F708.

[43] W. Yao, E. Croiset, Investigation of H_2, CO and syngas electrochemical performance using Ni/YSZ pattern anodes, ECS Trans. 53 (2013) 163–172.

[44] K. Eguchi, H. Kojo, T. Takeguchi, R. Kikuchi, K. Sasaki, Fuel flexibility in power generation by Solid Oxide Fuel Cells, Solid State Ionics 152 (2002) 411–416.

[45] J. Hanna, W. Lee, Y. Shi, A. Ghoniem, Fundamentals of electro-and thermochemistry in the anode of Solid Oxide Fuel Cells with hydrocarbon and syngas fuels, Prog. Energy Combust. Sci. 40 (2014) 74–111.

[46] J. Mizusaki, H. Tagawa, T. Saito, T. Yamamura, K. Kamitani, K. Hirano, S. Ehara, T. Takagi, T. Hikita, M. Ippommatsu, et al., Kinetic studies of the reaction at the nickel pattern electrode on YSZ in H_2/H_2O atmospheres, Solid State Ionics 70 (1994) 52–58.

[47] A. Bieberle, L. Meier, L. Gauckler, The electrochemistry of Ni pattern anodes used as Solid Oxide Fuel Cell model electrodes, J. Electrochem. Soc. 148 (2001) A646–A656.

[48] W. G. Bessler, M. Vogler, H. Störmer, D. Gerthsen, A. Utz, A. Weber, E. Ivers-Tiffée, Model anodes and anode models for understanding the mechanism of hydrogen oxidation in Solid Oxide Fuel Cells, Phys. Chem. Chem. Phys. 12 (2010) 13888–13903.

[49] L. Zhang, F. Liu, K. Brinkman, K. L. Reifsnider, A. V. Virkar, A study of gadolinia-doped ceria electrolyte by electrochemical impedance spectroscopy, J. Power Sources 247 (2014) 947–960.

[50] X. Guo, W. Sigle, J. Maier, Blocking grain boundaries in yttria-doped and undoped ceria ceramics of high purity, J. Am. Ceram. Soc. 86 (2003) 77–87.

[51] W. Jung, J. O. Dereux, W. C. Chueh, Y. Hao, S. M. Haile, High electrode activity of nanostructured, columnar ceria films for solid oxide fuel cells, Energy Environ. Sci. 5 (2012) 8682–8689.

[52] W. C. Chueh, Y. Hao, W. Jung, S. M. Haile, High electrochemical activity of the oxide phase in model ceria-Pt and ceria-Ni composite anodes, Nat. Mater. 11 (2012) 155–161.

[53] C. Li, Y. Sakata, T. Arai, K. Domen, K.-i. Maruya, T. Onishi, Carbon monoxide and carbon dioxide adsorption on cerium oxide studied by fourier-transform infrared spectroscopy. part 1. formation of carbonate species on dehydroxylated CeO2, at room temperature, J. Chem. Soc., Faraday Trans. 1 F 85 (1989) 929–943.

[54] K. R. Hahn, M. Iannuzzi, A. P. Seitsonen, J. r. Hutter, Coverage effect of the CO_2 adsorption mechanisms on CeO_2(111) by first principles analysis, J. Phys. Chem. C 117 (2013) 1701–1711.